applied sciences

MDPI

Review

Fiber Bragg Grating-Based Optical Signal Processing: Review and Survey

María R. Fernández-Ruiz [1,*,†] and Alejandro Carballar [2,*,†]

[1] Departamento de Electrónica, Universidad de Alcalá, 28805 Alcalá de Henares, Spain
[2] Departamento de Ingeniería Electrónica, Universidad de Sevilla, 41092 Sevilla, Spain
* Correspondence: rosario.fernandezr@uah.es (M.R.F.-R.); carballar@us.es (A.C.)
† These authors contributed equally to this work.

Abstract: This paper reviews the state of the art of fiber Bragg gratings (FBGs) as analog all-optical signal processing units. Besides the intrinsic advantages of FBGs, such as relatively low cost, low losses, polarization insensitivity and full compatibility with fiber-optic systems, they have proven to deliver an exceptional flexibility to perform any complex band-limited spectral response by means of the variation of their physical parameters. These features have made FBGs an ideal platform for the development of all-optical broadband filters and pulse processors. In this review, we resume the main design algorithms of signal processors based on FBGs, and we revisit the most common processing units based on FBGs and the applications that have been presented in the literature.

Keywords: optical signal processing; pulse shaping; fiber Bragg gratings; design methods; synthesis algorithms; ultrafast photonic processors

Citation: Fernández-Ruiz, M.R.; Carballar, A. Fiber Bragg Grating-Based Optical Signal Processing: Review and Survey. *Appl. Sci.* **2021**, *11*, 8189. https://doi.org/10.3390/app11178189

Academic Editor: Detlef Kip

Received: 28 July 2021
Accepted: 31 August 2021
Published: 3 September 2021

1. Introduction

The discovery of fiber Bragg gratings (FBGs) about four decades ago entailed a revolution in the field of telecommunications [1]. FBGs appeared as an all-optical device component capable of performing signal processing with low loss, relatively low cost and full-compatibility with fiber optic systems. FBGs immediately attracted much of researchers' attention, being a fruitful field of research with widespread application in a number of scientific and industrial fields [2–4]. FBGs are considered as basic building blocks in photonic circuits aimed at ultrafast information transmission and computing, as they deliver broadband operation (even greater than 1 THz) while avoiding inefficient electro-optical and opto-electronic (EO/OE) conversions [5].

A Bragg grating in a light-guiding medium such as an optical fiber is a periodic perturbation of its refractive index, causing certain reflectance and phase change in a wavelength range nearby that accomplishing the Bragg condition, i.e., $\lambda_B = 2\pi\Lambda$, where λ_B is the Bragg wavelength and Λ is the period of the refractive index perturbation [6].

Nowadays, two of the more prominent areas of application of FBGs are optical sensing [7,8] and optical signal processing [9,10]. In optical sensing, the Bragg wavelength of FBGs is highly sensitive to variations in temperature and strain, offering a precise transducer to these effects. This fact, together with their low weight, low size, easiness to multiplex and easiness to embed fiber in different materials have made FBG a widespread photonic sensing solution of high interest in an increasing number of fields such as civil engineering, medicine, aerospace, and more [11–16]. As optical signal processors, FBGs operate as broadband, linear filtering devices. In the 2000s, the versatility of FBGs to implement any desired linear filtering operation (bandpass, bandstop, customized phase filtering, etc.) was unveiled [6]. For this purpose, FBG design techniques consisting in engineering the apodization profile (i.e., the envelope of the periodic refractive index modulation of the fiber) and/or the grating period were developed. Hence, different types of optical filters and optical signal processing units (such as differentiators, integrators, pulse shapers,

etc.) were implemented with bandwidths ranging from tens of GHz to THz [17]. Recently, the rapid growth of semiconductor technologies and silicon-based photonics integrated circuits (PICs) has speeded up the interest in translating the functionalities attained by FBGs to integrated platforms (i.e., the so-called waveguide Bragg gratings), aimed at the realization of entire functionalities on a chip [18–20]. Besides, recent prospects foster a low cost for massive production using CMOS technology.

In this review, we focus on the application of FBG as signal processing units. First, we review the algorithms employed to analyze and synthesize FBG as linear filters, from approximate methods to "exact" analytical solutions. Then, we revisit the research on signal processors based on FBG carried out in the past two decades, discussing the design methodology employed and their applications. Finally, we provide insight for potential future lines of work in this area.

2. Review of Design Methods for Fiber Bragg Gratings

Fiber Bragg Gratings (also known as short-period gratings) are distributed reflectors that couple light from a forward-propagating core-mode ($E^+(z,f)$), to the same counter-propagating mode ($E^-(z,f)$) in an optical fiber, as represented in Figure 1. For simplicity, single mode operation can be generally assumed, since a single co- and counter-propagating mode intervenes in the coupling process [6]. This coupling dominates at a particular wavelength, specified by the grating period (typically in the sub-micrometer) via the Bragg phase-matching condition [6]. Mathematically, an FBG can be modeled as the modulation of the effective refractive index of the guided mode of interest along the fiber length z as:

$$n_{FBG}(z) = n_{eff}(z) + \Delta n(z) \cdot \cos\left(\int_0^z \frac{2\pi}{\Lambda(z')} dz'\right) \quad (1)$$

where $n_{eff}(z)$ is the effective refractive index for the fundamental mode, $\Delta n(z)$ is the apodization profile, i.e., the envelope of the refractive index modulation, $\Lambda(z)$ is the period variation (also defined as the chirp function) along the grating length, which is assumed to be L (Figure 1).

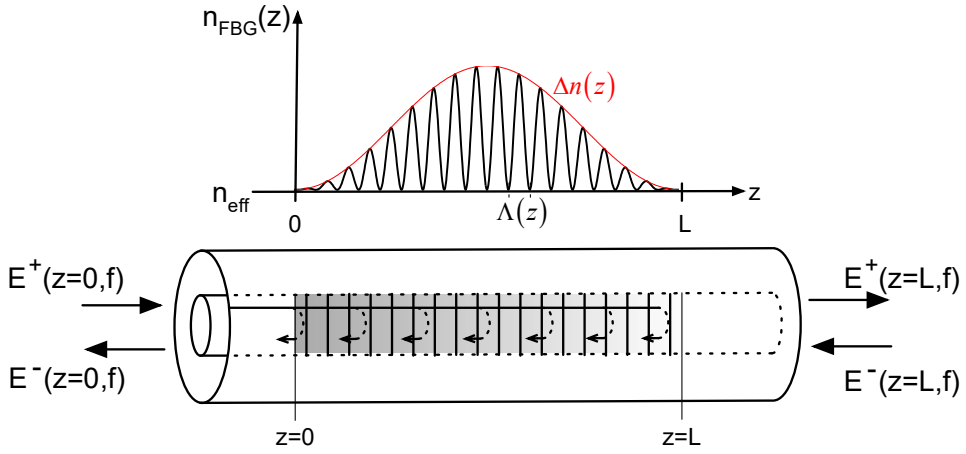

Figure 1. Nomenclature for the parameters of an arbitrary FBG of length L and for the electromagnetic optical fields at the two extremes (the grating period of the perturbation has been increased for illustrative purposes).

As previously mentioned, FBGs behave as linear, passive filters. They have a linear and time invariant (LTI) spectral response and hence, diverse signal processing functions can be generated by using techniques from Fourier analysis [21]. FBGs can work in both reflection and transmission, depending on whether the target output is attained at the same fiber end where the input is launched or in the opposite end. Their frequency responses (or

spectral transfer functions) in reflection and transmission, $H_R(f)$ and $H_T(f)$, respectively, and the corresponding temporal impulse responses, $h_R(t)$ and $h_T(t)$ are defined as:

$$H_R(f) = \left.\frac{E^-(z=0,f)}{E^+(z=0,f)}\right|_{E^-(z=L,f)=0}; h_R(\mathrm{t}) = \Im^{-1}[H_R(f)] \tag{2}$$

$$H_T(f) = \left.\frac{E^+(z=L,f)}{E^+(z=0,f)}\right|_{E^-(z=L,f)=0}; h_T(\mathrm{t}) = \Im^{-1}[H_T(f)] \tag{3}$$

where $\Im^{-1}$ denotes inverse Fourier transformation, t is the time variable, and f is the optical frequency variable. The spectral response of the grating in reflection and transmission, also defined as reflective and transmissive field coefficients, are generally complex functions. Along this work, we will define these spectral responses as $H_R(f) = |H_R(f)| \cdot \exp\{j\phi_R(f)\}$ and $H_T(f) = |H_T(f)| \cdot \exp\{j\phi_T(f)\}$, respectively. The reflectivity of the FBG is then obtained as $R(f) = |H_R(f)|^2$, while the transmissivity is $T(f) = |H_T(f)|^2$.

In linear regime, the reflective coefficient of an FBG acts as an optical band-pass filter, while the transmissive coefficient defines a band-stop filter. When operating in reflection, FBGs offer an extraordinary flexibility to achieve almost any desired complex-valued spectral filtering response, fundamentally constrained by practical fabrication limitations. In transmission, however, their response is minimum-phase [22], i.e., the imaginary part, $\mathrm{Im}[H_T(f)]$ of the FBG's spectral response in transmission is uniquely determined by the real part, $\mathrm{Re}[H_T(f)]$ through the Kramers-Kronig relationship [23,24]. To achieve a user-defined spectral response, the Bragg grating can be engineered, e.g., by changing its length L, modulating its envelope, $\Delta n(z)$, or modulating its grating period, $\Lambda(z)$ [6]. Researchers have intensively worked on the development of algorithms that predict the reflective and transmissive spectral responses, $H_R(f)$ and $H_T(f)$, from the refractive index profile $n_{FBG}(z)$ of the grating, and vice versa, i.e., algorithms that determine the $n_{FBG}(z)$ that would lead to a desired $H_R(f)$ or $H_T(f)$. These algorithms are known as analysis [25–33] and synthesis algorithms [34–42], respectively.

For the development of the FBG design algorithms, two hypotheses are to be considered. First, the refractive index modulation, $n_{FBG}(z)$, is regarded as a one-dimensional parameter. Secondly, the electric fields propagating along the grating, $E^+(z,f)$ and $E^-(z,f)$, are assumed to be ideal monochromatic plane waves. In this Section, we briefly describe the existing algorithms with special emphasis in the more precise solutions, which are nowadays widely employed in the design of efficient FBG-based optical signal processors.

2.1. Approximate Methods

Before exact analytical solutions to the analysis and synthesis of FBGs were developed (around the 2000s), the parameters of the grating were engineered to achieve the target functionality based on approximations. A well-known approximation to that end is the first-order Born approximation [26], which relies on the use of weak-coupling gratings.

2.1.1. First-Order Born Approximation

The first-order Born approximation has been used as a grating design tool to either determine the grating amplitude and phase profiles required to obtain a target reflective spectral response $H_R(f)$, or to anticipate the $H_R(f)$ that will produce a certain grating profile. In particular, this approximation establishes that under weak-coupling conditions (i.e., when the maximum reflectivity is $\max[R(f)] = R_{\max} \ll 1$), an estimation of the reflective impulse response of an FBG, $h_{R,est}(t)$, is directly related to the spatial profile of the refractive index perturbation, $n_{FBG}(z)$, by [26]:

$$h_{R,est}(t) = \left.\frac{-\frac{dn_{FBG}(z)}{dz}}{2 \cdot n_{FBG}(z)}\right|_{z=\frac{t}{2}\cdot\frac{c}{n_{av}(z)}}; \; n_{av}(z) = \int_0^z n(z')dz' \tag{4}$$

where $n_{av}(z)$ is the average refractive index from the grating input to the location z, and c is the speed of light in a vacuum. Under the Born approximation, the estimation of the reflection impulse response, $h_{R,est}(t)$, is proportional to the spatial index-modulation profile of the grating in amplitude and phase. Therefore, the estimation for the reflection frequency response is directly obtained by:

$$H_{R,est}(f) = \Im[h_{R,est}(t)] \tag{5}$$

This simple approach can be readily employed to implement the analysis and synthesis of a wide variety of FBGs operating on waveforms with picosecond resolutions. However, this approximation starts to fail for strong-coupling gratings. The reason is that the Born approximation is strictly valid when $|\kappa|L \ll 1$, where κ is the coupling coefficient, which is proportional to the index modulation amplitude, i.e., $|\kappa| = \pi \cdot \Delta n/\lambda$ (λ is the wavelength). The parameter κ provides the relative amount of power coupled between two modes per unit length. Longer gratings are associated to weak Δn, since the coupling coefficient needs to be sufficiently low so that the electromagnetic field maintains certain magnitude to penetrate the full grating length.

2.1.2. Space-to-Frequency-to-Time Mapping

Another approach for the design of FBG-based optical signal processors based on the Born approximation was later presented, leveraging the space-to-frequency-to-time mapping [39].

This technique consists of designing the apodization function of a linearly chirped FBG, working in the weak-coupling regime (i.e., $|\kappa|L \ll 1$). If the grating's chirp induced dispersion $\ddot{\Phi}(s^2)$, defined as $\ddot{\Phi} = \partial^2\phi_R(t)/\partial t^2$, accomplishes that $\ddot{\Phi} \gg {\Delta t_1}^2/8\pi$, with Δt_1 being the temporal duration of the impulse response for the optical signal processor, a time-to-frequency mapping occurs. Then, the amplitude of the impulse response in reflection, $h_R(t)$, is proportional to the amplitude of the reflective field coefficient of the filter, $H_R(f)$. Additionally, by operating under the Born approximation, there is a space-to-frequency mapping process, in which the magnitude of $H_R(f)$ is approximately proportional to $\Delta n(z)$.

Consequently, in this situation, the amplitude of the grating apodization profile directly determines the magnitude of both the grating's impulse response and the spectral transfer function. A waveform proportional to the target temporal -or spectral- response only needs to be spatially "recorded" in the apodization mask to be employed in the grating writing process. Since it works under the Born approximation, this grating design technique presents the same limitation in energy efficiency (related to the required low reflectivity) as the previous one here described. Besides, the use of a linearly chirped FBG imposes a quadratic phase in the reflective spectral response, limiting the applicability of this approach to amplitude-only optical signal processors. On the other hand, the processing bandwidth is restrained to tens of GHz, limited by the physically attainable fiber-grating length, which is typically shorter than ~40 cm.

The general design of FBGs as optical signal processors, including high-reflectivity gratings (leading to increased energy efficiency), involves the use of more exact analysis and synthesis algorithms, which are described in what follows.

2.2. Analysis of Fiber Bragg Gratings

The analysis of FBGs provides the reflection $H_R(f)$ and transmission $H_T(f)$ spectral responses obtained from a particular grating structure, $n_{FBG}(z)$. In this section, we describe analytically the Coupled Mode Theory and Multilayer methods for the analysis of FBGs.

2.2.1. Coupled-Mode Theory (CMT)-Based Analysis Method

The Coupled-mode theory is a widespread technique that relates counter-propagating electromagnetic waves within the grating structure using coupled differential equations [25,27,28]. CMT directly provides an analytic solution for the propagation of the

electromagnetic fields through a uniform FBG, which is a grating with constant $\Delta n(z)$ and $\Lambda(z)$ along its length. In particular,

$$n_{FBG}(z) = n_{eff} + \Delta n_{\max} \cdot \cos\left\{\frac{2\pi}{\Lambda}\right\} \tag{6}$$

where n_{eff}, $\Delta n_{\max}$ and Λ are all constant values. The reflective and transmissive coefficients of the uniform FBG are given by [6,27]:

$$H_R(f) = \frac{-j\kappa^* \sinh(\kappa L)}{\gamma \cosh(\kappa L) + j(\Delta\beta/2)\sinh(\kappa L)} \tag{7}$$

$$H_T(f) = \frac{\gamma \cdot \exp(-j\beta_0 L)}{\gamma \cosh(\kappa L) + j(\Delta\beta/2)\sinh(\kappa L)} \tag{8}$$

where $*$ stands for complex conjugation, the optical waveforms $E^+(z,f)$ and $E^-(z,f)$ involved in these expressions are defined in Figure 1, the propagation constant is $\beta_0 = \pi/\Lambda$, and γ is defined as $\gamma = |\kappa|^2 - (\Delta\beta/2)^2$. The parameter $\Delta\beta = \beta - \beta_0$. The coupling coefficient κ is defined as $\kappa = -j\pi f \Delta n_{\max}/c$.

Now, let us assume the analysis of a non-uniform FBG. The induced refractive index can be expressed following Equation (1). In this equation, we have written the phase of the refractive index modulation as a function of the grating period variation ($\Lambda(z)$). In this case, the coupling coefficient varies along the grating's length and is given by:

$$\kappa(z) = -j\frac{\pi f \Delta n(z)}{c} \exp\left\{-j2\pi \int_0^z \left(\frac{1}{\Lambda(z')} - \frac{1}{\Lambda_0}\right) dz'\right\} \tag{9}$$

where Λ_0 is a specific grating period for reference.

The CMT-based algorithm leverages the transfer-matrix method (TMM) to implement a discretization process of a non-uniform grating [31,33], as shown in Figure 2. Thus, the entire grating is split into N layers of length δL_i, with $i \in [1, N]$, each of them containing few periods. In each layer, we assign constant values to the parameters γ, κ and $\Delta\beta$, e.g., by selecting their values at the center of the section. Hence, the different grating layers are approximated as uniform structures [2,27], which can be readily described by the transfer matrix of a uniform FBG [6,27] of length δL_i, i.e.,

$$\begin{bmatrix} E^+(z_i,f) \\ E^-(z_i,f) \end{bmatrix} = \begin{bmatrix} M_{i,11}(f) & M_{i,12}(f) \\ M_{i,21}(f) & M_{i,22}(f) \end{bmatrix} \begin{bmatrix} E^+(z_i+\delta L_i,f) \\ E^-(z_i+\delta L_i,f) \end{bmatrix} = [M_{U,i}] \begin{bmatrix} E^+(z_i+\delta L_i,f) \\ E^-(z_i+\delta L_i,f) \end{bmatrix} \tag{10}$$

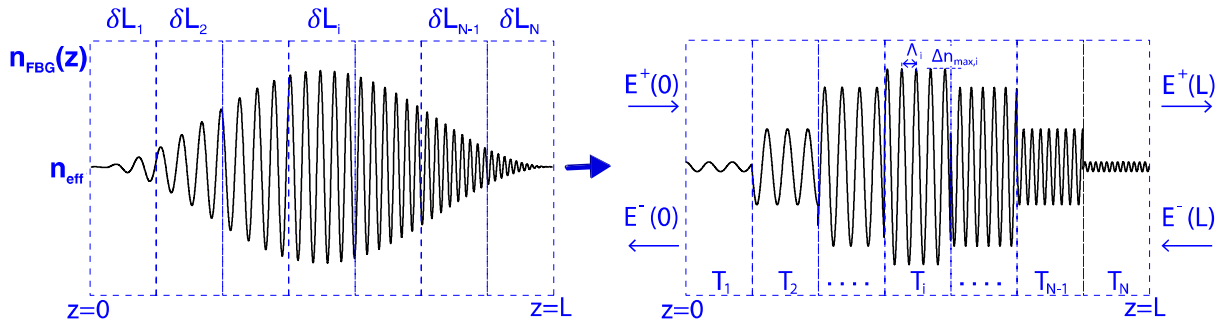

Figure 2. Representation of the division of a non-uniform FBG into layers that are approximated by uniform FBG. The resulting structure can be readily analyzed via CMT and TMM. The dependence of propagating waves with the optical frequency is omitted for the sake of simplicity.

The elements of the matrix $M_{U,i}$ are derived from the CMT as

$$M_{i,11}(f) = \frac{\gamma \cosh(\gamma \cdot \delta L_i) + j(\Delta\beta/2)\sinh(\gamma \cdot \delta L_i)}{\gamma} \exp(j\beta_0 \cdot \delta L_i) \tag{11}$$

$$M_{i,12}(f) = \frac{j\kappa \sinh(\gamma \cdot \delta L_i)}{\gamma} \exp(-j\beta_0 \cdot \delta L_i) \tag{12}$$

$$M_{i,21}(f) = \frac{j\kappa^* \sinh(\gamma \cdot \delta L_i)}{\gamma} \exp(j\beta_0 \cdot \delta L_i) \tag{13}$$

$$M_{i,22}(f) = \frac{\gamma \cosh(\gamma \cdot \delta L_i) - j(\Delta\beta/2)\sinh(\gamma \cdot \delta L_i)}{\gamma} \exp(-j\beta_0 \cdot \delta L_i) \tag{14}$$

Eventually, the total grating response is obtained by multiplying the matrices of the different layers in the appropriate order:

$$[M_{FBG}] = [M_{U,1}] \cdot [M_{U,2}] \cdot \ldots \cdot [M_{U,i}] \cdot \ldots \cdot [M_{U,N-1}] \cdot [M_{U,N}] \tag{15}$$

The grating's reflection and transmission spectral responses are obtained as:

$$H_R(f) = \left.\frac{E^-(z=0,f)}{E^+(z=0,f)}\right|_{E^-(z=L,f)=0} = \frac{M_{FBG,21}(f)}{M_{FBG,11}(f)} \tag{16}$$

$$H_T(f) = \left.\frac{E^+(z=L,f)}{E^+(z=0,f)}\right|_{E^-(z=L,f)=0} = \frac{1}{M_{FBG,11}(f)} \tag{17}$$

The number of layers (N) selected to implement the piecewise calculation is established by the required accuracy. However, it is important to note that the section lengths must accomplish that $\delta L_i \gg \Lambda_{\max}$, with $\Lambda_{\max}$ the longer period found along the grating. Otherwise, the approximations considered in the CMT to attain Equations (7) and (8) will start to fail [6,27]. This analysis method delivers an accurate outcome for the broad majority of FBGs of practical interest, i.e., those containing an arbitrary apodization profile, arbitrary period profile and even those including phase shifts, with relatively low computational time. For gratings incorporating phase shifts in their period, also known as phase-shifted gratings [6], a phase-shift matrix $[M_{ps,i}] = \begin{bmatrix} \exp\{j\phi_p/2\} & 0 \\ 0 & \exp\{-j\phi_p/2\} \end{bmatrix}$ is to be inserted in the adequate location in Equation (15), where ϕ_p is the shift in the phase of the refractive index modulation [6]. Yet, CMT-TMM is not valid for the analysis of specific grating profiles including superimposed FBGs or gratings based on superstructures.

2.2.2. Multilayer-Based Analysis Method

The algorithm of multi-layer (ML) represents an accurate solution to analyze any arbitrary FBG. ML-based algorithm also leverages the transfer-matrix method [31,33]. In this case, ML-TMM sections the whole grating into layers whose length δl_i is sufficiently short so that the refractive index variation within the layer can be regarded as constant. Typically, $\delta l_i \ll \Lambda_{\min}$, with $\Lambda_{\min}$ being the shorter period in the grating [29,30] (see Figure 3).

The resulting arrangement can be seen as a multi-layer structure that alternates two elements, namely, a dielectric medium of constant refractive index and the interface between two dielectric media of different refractive indexes. Considering the propagation of a plane wave, the transfer matrix that characterizes a lossless medium with constant refractive index n_i and length δl_i is

$$[M_{M,i}] = \begin{bmatrix} \exp(jk_0 n_i \cdot \delta l_i) & 0 \\ 0 & \exp(-jk_0 n_i \cdot \delta l_i) \end{bmatrix} \tag{18}$$

where $k_0 = 2\pi f/c$ is the wavenumber in a vacuum.

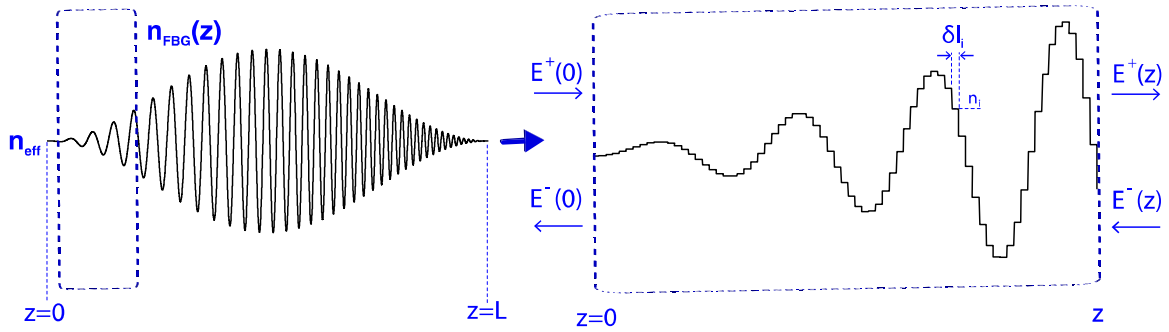

Figure 3. Representation of the division of a non-uniform FBG into layers suitable for the analysis using ML-TMM. The dependence of waves with the optical frequency is omitted for simplicity.

Assuming normal incidence on an interface between two dielectric media of different refractive indexes n_i and n_{i+1}, the transfer matrix of this interface is [29,30]:

$$[M_{I,i}] = \frac{1}{2n_i}\begin{bmatrix} n_i + n_{i+1} & n_i - n_{i+1} \\ n_i - n_{i+1} & n_i + n_{i+1} \end{bmatrix} \tag{19}$$

Hence, the transfer matrix of the whole grating M_{FBG} can be obtained from the multiplication of the 2 × 2-transfer matrices characterizing the sequence of those simpler elements, as

$$[M_{FBG}] = [M_{I,1}] \cdot [M_{M,1}] \cdot \ldots \cdot [M_{I,i}] \cdot [M_{M,i}] \cdot \ldots \cdot [M_{I,N}] \cdot [M_{M,N}] \cdot [M_{I,N+1}] \tag{20}$$

The first and last transfer matrices characterize the interface between the unperturbed fiber core and the first/last layer of the grating. Finally, the grating's reflection and transmission spectral responses $H_R(f)$ and $H_T(f)$ are readily obtained from the elements of M_{FBG} using the Equations (16) and (17). As previously stated, ML-TMM is a general algorithm useful for the characterization of any arbitrary grating profile, including a non-cosenoidal or even non-periodic refractive index perturbation. However, due to the required high sampling rate, the computation workload required in ML-TMM becomes extremely heavy for FBGs longer than a few cm.

2.3. Synthesis of Fiber Bragg Gratings from a Targeted Reflection Specifications

The design of FBG generally starts from the specifications of the target reflective spectral response $H_R(f)$ and pursue the generation of the refractive index modulation (Equation (1)) required to produce such response. This problem is generally known as the inverse scattering or grating synthesis problem [34].

2.3.1. CMT-Based Synthesis Method

The synthesis method based on CMT delivers the local coupling coefficient $\kappa(z)$ from the specification of the target reflection spectral response $H_R(f)$. As previously seen, the resulting $\kappa(z)$ provides the needed information to write the grating structure on the fiber, i.e., the refractive index envelope $\Delta n(z)$ and the period variation $\Lambda(z)$ (see Equation (9)). This method has a straightforward description, since it makes use of the direct solution of exactly the same coupled-mode equations of the grating analysis [35–37].

Once again, the propagation problem has to be discretized. Hence, the entire grating is virtually divided in a series of N sections of length δL, which shall be modeled by uniform FBGs. N is selected so that each section contains several periods, $\delta L \gg \Lambda_0$ (recall that the grating period for reference, Λ_0, can be obtained from the central frequency of the target spectral response and the Bragg condition). The transfer matrix of a uniform Bragg grating

is $M_{U,i}$, which is given by Equations (11)–(14). The fields before the first section ($z_1 = 0$) are given by [36]:

$$\begin{bmatrix} E^+(z=0,f) \\ E^-(z=0,f) \end{bmatrix} = \begin{bmatrix} 1 \\ H_R(f) \end{bmatrix} \tag{21}$$

From the matrix $M_{U,i}$, it is possible to define a discrete, complex reflection coefficient associate to each segment, which is related to the coupling coefficient as [37]

$$\rho = -\tanh(|\kappa|L)\frac{\kappa^*}{\kappa} \tag{22}$$

From Fourier analysis, we know that the reflection coefficient of the first layer is

$$\rho_1 = h_R(t=0) = \frac{1}{N}\int_0^\infty H_R(f)df \tag{23}$$

The reason is that the impulse response for $t = 0$ coincides with the case where only the first reflector is present. The coupling coefficient of the first layer κ_1 is obtained from Equation (23). At this point, we can generate the first matrix $M_{U,1}$, which provides information of the grating structure from $z = 0$ to $z = \delta L$. The spectral response yielded from the remaining grating is obtained by substituting Equation (21) into Equation (10), and calculating [36]

$$H_R^{zL}(f) = \frac{E^-(z=\delta L,f)}{E^+(z=\delta L,f)} = \frac{-M_{U,1,21} + M_{U,1,11}\cdot H_R(f)}{M_{U,1,22} - M_{U,1,12}\cdot H_R(f)} \tag{24}$$

Next, the reflection coefficient of the next layer is obtained following the same reasoning as in Equation (23), using the spectral response of the remaining grating structure $H_R^{zL}(f)$,

$$\rho_2 = \frac{1}{N}\int_0^\infty H_R^{zL}(f)df \tag{25}$$

These steps are employed successively until the entire grating structure is determined. This algorithm embodies a computationally efficient layer-peeling algorithm for the design of the broad majority of fiber gratings of practical interest, including long gratings (e.g., tens of cm).

2.3.2. ML-Based Synthesis Method

The ML-TMM-based synthesis algorithm offers the advantages of generality and accuracy over the previously described CMT-based method. This method delivers the required refractive index profile, $n_{FBG}(z)$, (instead of the coupling coefficient) from the specified response in reflection. Its high sampling rate makes this method a practical tool to synthesize gratings with discontinuities or local defects of the order of the local period, or even to detect defects in a fabricated device.

In particular, the spatial resolution of the recovered local refractive index $n_{FBG}(z)$ is below the local period ($\delta l \ll \Lambda$) [29,30]. This minimum discretization step impedes working with an equivalent low-pass spectral response, forcing us to work with a spectral response $H_R(f)$ defined from $f = 0$ to $f = c/\left(4n_{eff}\delta l\right)$. The maximum value of the optical frequency is given by the sampling rate of the impulse response of the grating in reflection, Δt, which is equal to half the round-trip delay in a layer of length δl, $\Delta t = n_{eff}\delta l/c$ (see Figure 4a). The sampled reflection impulse response, $h_{RS}(p)$ (targeted reflection specifications) is obtained as:

$$h_R(t) = \Im^{-1}\{H_R(f)\} = \sum_{p=0}^{\infty} h_{RS}(p)\cdot\delta(t-2p\Delta t) \tag{26}$$

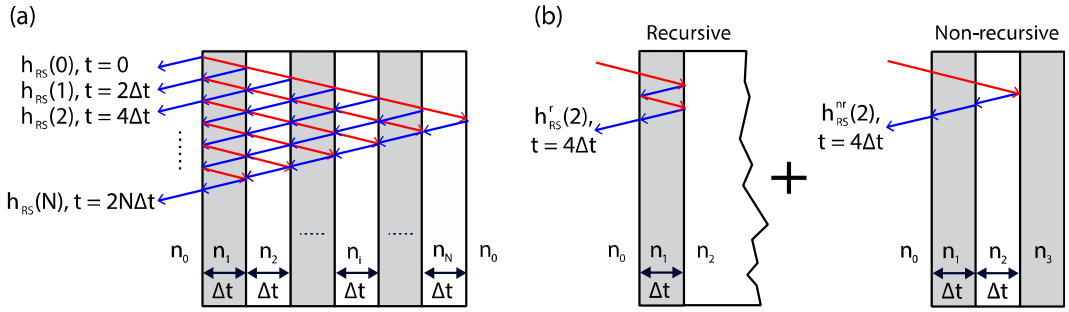

Figure 4. (**a**) Scheme of the division into layers of the FBG and the space-time paths contributing to the total sampled impulse response; (**b**) Decomposition of the space-time paths into the recursive path and the non-recursive path. The value of the refractive index of each layer is calculated from the non-recursive component of the impulse response in that layer, where the total impulse response and the non-recursive component are known.

The steps to obtain the required grating's refractive index modulation are the following [35]. Let us assume n_0 as the refractive index of the unperturbed waveguide. The value of n_1 is calculated from the first sample of the impulse response $h_{RS}(0)$:

$$n_1 = n_0\left(\frac{1-h_{RS}(0)}{1+h_{RS}(0)}\right) \tag{27}$$

Observing Figure 4a, we have that

$$h_{RS}(1) = t_{01}\cdot r_{12}\cdot t_{10} \tag{28}$$

where t_{xy} and r_{xy} represent the field transmission and reflection coefficients (respectively) for the transition between the dielectric media x and y, assuming normal incidence. The coefficient r_{12} can be then calculated from the sampled impulse response in reflection as

$$r_{12} = \frac{h_{RS}(1)}{t_{01}\cdot t_{10}} = \frac{(n_0+n_1)^2 h_{RS}(1)}{4n_0n_1} \tag{29}$$

The refractive index in the second layer n_2 is obtained as

$$n_2 = n_1\left(\frac{1-r_{12}}{1+r_{12}}\right) \tag{30}$$

As represented in Figure 4b, it must be noted that, from the third coefficient of the sampled impulse response, $h_{RS}(2)$, $h_{RS}(p)$ can be split into a recursive contribution (left part) and a non-recursive one (right part) [35]. The non-recursive part can be written as

$$h^{nr}_{RS}(2) = t_{01}t_{12}r_{23}t_{21}t_{10} = r_{23}\prod_{i=0}^{1}\left(\frac{4n_in_{i+1}}{(n_i+n_{i+1})^2}\right) \tag{31}$$

where the only unknown factor is r_{23} which is needed to obtain n_3 since

$$n_3 = n_2\left(\frac{1-r_{23}}{1+r_{23}}\right) \tag{32}$$

Considering that the grating structure finishes at the second layer, i.e., the second layer is infinitely long; the recursive part $h^r_{RS}(2)$ can be readily calculated by applying the ML-TMM analysis technique. Then, r_{23} is obtained as

$$r_{23} = \frac{h^{nr}_{RS}(2)}{\prod_{i=0}^{1}\left(\frac{4n_in_{i+1}}{(n_i+n_{i+1})^2}\right)} = \frac{h_{RS}(2)-h^r_{RS}(2)}{\prod_{i=0}^{1}\left(\frac{4n_in_{i+1}}{(n_i+n_{i+1})^2}\right)} \tag{33}$$

From r_{23}, the value of n_3 is solved using Equation (32). This last step must be repeated until the last sample of $h_{RS}(N)$.

Of course, in the literature, we can find numerous references where variants of the here described approaches have been proposed [32,40]. Nevertheless, the described methods are found to have a straightforward, simpler description and are useful for any designer to implement any arbitrary optical filter based on FBG.

2.4. Synthesis of Fiber Bragg Gratings from a Targeted Transmission Specifications

Although FBGs mainly operates in reflection mode, FBGs working in transmission possess appealing advantages, such as the fact that no additional elements (e.g., an optical circulator) are required to detach the grating output from the input signal, hence reducing the cost and size of the processor unit. Besides, FBGs operating in transmission are more robust against errors induced in the fabrication process. This is due to the weak interaction between the propagating electromagnetic field and the grating when the electromagnetic field is simply transmitted. It has been observed that, in this case, imperfections in the grating structure are not "impressed" on the propagating wave [38]. On the other hand, the processing bandwidth of transmissive FBGs has been found to reach more than one order of magnitude that attained by reflective configurations. In reflection, the device bandwidth is restricted by the attainable spatial resolution of grating fabrication technologies for tailoring the apodization profile. To give a quantitative example, if the apodization profile is written with sub-millimeter resolution (which is typically feasible), the resulting FBG is limited to temporal resolutions of several picoseconds. In terms of spectral bandwidth, this corresponds to a few hundreds of GHz [5]. As explained in this section, FBGs in transmission permit a relaxation of the spatial resolution of the attainable grating apodization profile in a tailored fashion, enabling the synthesis of THz-bandwidth signal processors.

The synthesis process for a targeted FBG operating in transmission starts from the specification of the target transmissive coefficient, $H_T(f)$, (it may also start from the specification of the required transmission impulse response, $h_T(t)$), and must produce the required refractive index perturbation.

2.4.1. Minimum-Phase Transmissive Transfer Function

As previously mentioned, the transmission spectral response of an FBG is necessarily minimum-phase (MP). In addition, as per the principle of conservation of energy, the transmissivity and reflectivity must accomplish $T(f) = 1 - R(f)$. In this scenario, the given specifications of $|H_T(f)|$ directly determine $\phi_T(f)$ and $|H_R(f)|$. Hence, the design problem reduces to the synthesis of an FBG whose reflection amplitude spectral response is $|H_R(f)|$, while the reflection spectral phase $\phi_R(f)$ appears as a degree of freedom to achieve the simplest grating implementation [38,41]. For instance, if a quadratic spectral phase is considered (i.e., a linear chirp), the FBG reflection spectral response to be synthesized can be mathematically expressed by [41]:

$$H_R(f) = W(f)\sqrt{R_{\max}\left(1 - |H_T(f)|^2\right)} \cdot \exp\left\{j\left(\frac{1}{2}\beta_{d2}(2\pi f)^2 + (2\pi f)\tau_d\right)\right\} \tag{34}$$

where $R_{\max}$ is the maximum reflectivity; $\beta_{d2} = \ddot{\Phi}/L$ (s^2/m) is the slope of the group-delay as a function of the angular frequency per unit length; $W(f)$ is a windowing function employed to attain a band-pass response in reflection; and τ_d is a time delay introduced to produce a causal response. The parameter β_{d2} determines the minimum grating length L as

$$\beta_{d2} = \frac{n_{eff}L}{\pi Bc} \tag{35}$$

being B the full-width (e.g., at 99% of the maximum) reflection bandwidth of the device (Hz). Hence, β_{d2} is a fundamental design parameter, which can be suitably designated

to guarantee that the synthesized grating apodization has a resolution attainable by the available fabrication method.

From $H_R(f)$ given in Equation (34), which is obtained from targeted $|H_T(f)|$ specifications, the synthesis algorithms presented in Section 2.3 can be applied to obtain the desired $n_{FBG}(z)$. Results will show that a higher dispersion value, β_{d2}, leads to a more relaxed spatial resolution and a lower peak of the refractive index profile, at the cost of producing a longer device. In general, any optical processing functionality can be implemented using this configuration provided that its transfer function is minimum-phase [38]. The synthesized grating profile obtained from this design approach is much simpler than that obtained from previous approaches (based on space-to-time-to-frequency mapping [39]) and readily feasible, even for a strong coupling grating.

2.4.2. Non Minimum-Phase Transmissive Transfer Function

In principle, signal processors whose transfer functions are not a minimum-phase function, $H_{NMP}(f)$, would not benefit from the possibility of being implemented by an FBG operating in transmission. However, few years ago, a general approach was presented, capable of synthesizing any arbitrary linear optical pulse processor, including those requiring a non-MP filtering response, using a MP transfer function $H_{MP}(f)$ [42]. This approach relies on the property described and demonstrated in [24] that establishes that "any causal temporal function with a dominant peak around or close to the origin will be either a MP function or close to one". Hence, the presented design scheme starts from the target non-MP transmisive temporal impulse response, $h_{NMP}(t) = \Im^{-1}[H_{NMP}(f)]$, and converts it into a MP response by just introducing an instantaneous component, e.g., a Dirac delta function $\delta(t)$ [42], in the following fashion

$$h_{MP}(t) = K_1 \cdot \delta(t) + K_2 \cdot h_{NMP}(t - \tau_G) \tag{36}$$

where τ_G is the time delay between the two terms and $K_i, i = 1, 2$, are their amplitudes, which regulate the distribution of the input energy at the grating output. The corresponding spectral transfer function will be MP and can be expressed as

$$H_{MP}(f) = K_1 + K_2 \cdot H_{NMP}(f) \cdot \exp(-2\pi f \tau_G) \tag{37}$$

Note that Equation (37) defines an interferometric response where the phase of $H_{NMP}(f)$ is encoded in the phase of the resulting cosine-like spectral shape (a particular example of the described spectral profile is shown later in Section 3.4). $H_{MP}(f)$ can be readily synthesized by following the algorithm presented in previous Section 2.4.1. Hence, $H_T(f)$ must approximate $H_{NMP}(f)$ over the grating operation bandwidth. The selection of the values of K_1 and K_2 is restrained by the grating physical constraints. First, the maximum transmissivity is limited to $T_{\max} = 1$ and hence [42]

$$|H_T(f)| \leq \sqrt{T_{\max}} \rightarrow K_1 + K_2 \leq 1 \tag{38}$$

Besides, the maximum reflectivity $R_{\max}$ attained imposes that

$$|H_T(f)| \geq \sqrt{1 - R_{\max}} \rightarrow K_1 - K_2 \leq \sqrt{1 - R_{\max}} \tag{39}$$

This inequality becomes strict when $R_{\max} = 1$ to avoid singular points in $H_{MP}(f)$. However, this situation is not usually attained in practice ($R_{\max} < 1$), and hence Equations (38) and (39) can be solved using the equal signs. This fact enables optimizing the energy transfer to the non-MP component of the output signal. Note that the maximum signal energy transferred to the non-MP portion will be of about 50%, attained when $R_{\max}$ approaches 1. The described approach can be applied provided that the target impulse response is restricted to a well-defined, finite temporal window.

3. Survey of Signal Processing Units based on FBGs

The development of the design tools described above, and especially the synthesis tools, triggered a vast development of linear optical signal processors based on FBGs. Since the FBG implements an LTI filter, the design of the targeted optical signal processor requires the knowledge of the spectral responses of both the input signal $X(f)$ and the target output $Y(f)$ [43]. Hence, the transfer function of the processor is determined by $H(f) = Y(f)/X(f)$, being the impulse response $h(t) = \Im^{-1}[H(f)]$, its inverse Fourier transform, as depicted in Figure 5.

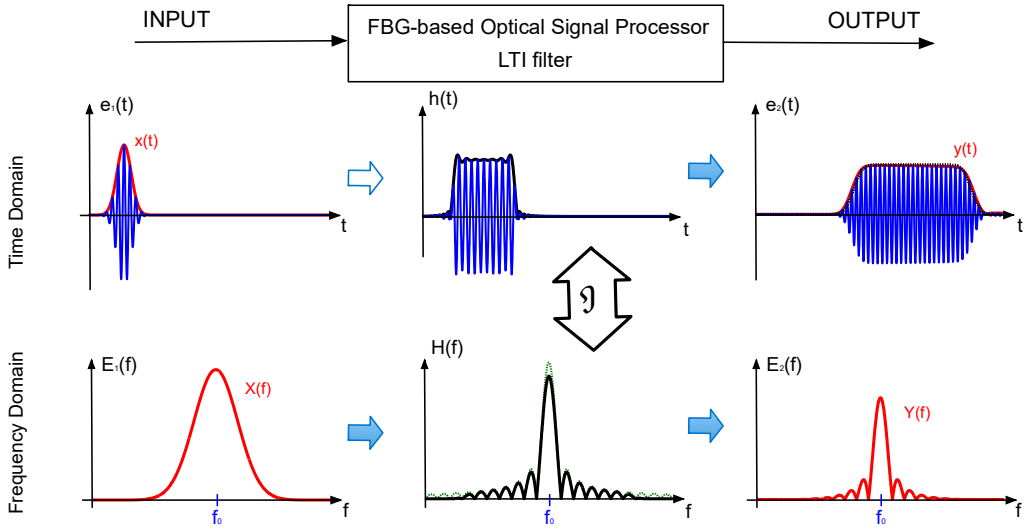

Figure 5. Diagram for the principle of operation of an FBG-based optical signal processor in both time and frequency domains. $e_i(t)$ and $E_i(f)$, with $i = 1, 2$, stand for optical fields in the time and frequency domain, respectively.

The performance of the FBG-based optical signal processor has been typically evaluated by three parameters [17]: the energy efficiency, the cross-correlation coefficient, C_C; and the Time-Bandwidth Product (TBP). The energy efficiency is obtained as the output-to-input waveform energy ratio. The C_C coefficient measures the processing error and is given by

$$C_C[\%] = \frac{\int_{-\infty}^{+\infty} y(t) \cdot y_{ideal}(t) \cdot dt}{\sqrt{\int_{-\infty}^{+\infty} y^2(t)dt} \cdot \sqrt{\int_{-\infty}^{+\infty} y_{ideal}^2(t)dt}} \times 100 \quad (40)$$

where $y(t)$ and $y_{ideal}(t)$ are the actual and ideal output waveforms, respectively. This C_C coefficient provides a precise estimation of the similarity between the obtained waveform and the ideal waveform, thus allowing calculating the TBP of the proposed design. Finally, the TBP is calculated as the ratio between the maximum and the minimum input pulse 3 dB-bandwidth with C_C higher than a fixed value, e.g., 95%.

In this section, we describe different signal processing units that have been presented in the literature along the past two decades, as well as the method employed for their design.

3.1. Amplitude and Phase Optical Filters

The straightforward application of FBGs is that of amplitude and/or phase optical filters. A very popular application of FBGs as an amplitude filter is that of add-and-drop optical multiplexers for DWDM systems [44]. For a finer selection/suppression of channels, the leading and trail edges of the grating spectral response should be as sharp as possible. This has led researchers to seek ways to efficiently suppress the typical lobes that appear in the spectral response of uniformly apodized FBGs (i.e., FBG with a rectangular-like refractive index envelope) [6]. Several proposals were reported based on analysis algorithms, based on particular apodization profiles such as Gaussian, hyperbolic

tangent, etc. [45]. Later, by means of synthesis algorithms, optical filters with rectangular-like amplitude spectral response and linear phase response (i.e., with no dispersion), were attained, which represent an optimized filter spectral response for add-and-drop multiplexers in ultra-dense DWDM systems [40,46,47].

As phase filters, linearly-chirped FBGs have been widely exploited for dispersion compensation. A linear variation of the grating period along its length translates into a linear group delay [48]. Nowadays, commercially available linearly-chirped FBGs modules are implemented to compensate for dispersion along several hundreds of km of G.652 fiber (i.e., conventional single-mode fiber) with very small form factor (e.g., Figure 6 shows the measured reflection spectral characteristic for a commercial linearly-chirped FBG).

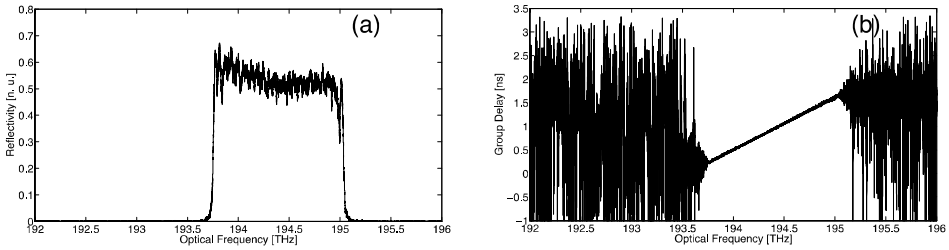

Figure 6. Measured reflection spectral characteristic of a typical linearly-chirped FBG: (**a**) Reflectivity versus optical frequency, and (**b**) reflection group delay with a linear slope of 1100 ps^2.

Finally, linearly-chirped FBGs have been also proposed as a real-time Fourier transformer [49], following the time-space duality [50]. Using the temporal analog of spatial Fraunhofer diffraction, the linearly-chirped FBG act as dispersive media in reflection mode, providing at its output a signal, $y(t)$, proportional to the Fourier transform of the input signal envelope, $x(t)$, at the angular frequency $\omega = t/\ddot{\Phi}$:

$$y(t) \propto \{\Im[x(t)]\}_{\omega=t/\ddot{\Phi}} \tag{41}$$

where $\ddot{\Phi}$(s^2) is the dispersion coefficient for the linearly-chirped FBG (i.e., the linear group delay as a function of the angular frequency). The FBG-based real-time Fourier transformer constitutes a key component for creating time-domain equivalents of well-known spatial optical signal processing systems [51].

3.2. Optical Differentiators

An optical differentiator obtains the derivative of the complex envelope of an input optical signal [52]. Therefore, the transfer function of an arbitrary order differentiator can be written as

$$y(t) \propto \frac{d^N x(t)}{dt^N} \rightarrow H_{diff}(f) \propto (j \cdot (f - f_0))^N \tag{42}$$

where j is the imaginary unit and N is the differentiator order. Applications of optical differentiators in the literature include the generation of arbitrary-order Hermite-Gaussian (HG) optical pulses [53], which can be employed as advanced coding for network access applications. Besides, optical differentiators can be applied for solving differential equations (ODEs) in analog computing systems. These equations play a fundamental role in practically any field of science or engineering, and the possibility of performing these computations all-optically implies potential processing speeds well beyond the reach of present electronic computing systems [5].

Several approaches for first- and high-order optical differentiators have been proposed in the literature based on FBGs, providing either different operation bandwidth or spectral resolution, still within the practical limitations of the technology [52–63]. First approaches proposed multiple-phase-shifts FBGs operating in reflection for first- and high-order differentiation, but with a limited bandwidth around 20 GHz [54,55]. Afterwards, an alternative design approach based on the use of especially apodized linearly-chirped FBG operated

in transmission (following the space-to-frequency-to-time mapping design method) were proposed and experimentally demonstrated increasing the operation bandwidths to a few hundreds of GHz [56,57,60].

Finally, optical differentiators have been also proposed in a transmissive configuration based on synthesis algorithms, as $H_{diff}(f)$ is a minimum-phase function. A first-order all-optical differentiator with a 2 THz bandwidth (full-width at 0.1% of the maximum amplitude) has been designed using a linearly chirped FBG and following the synthesis algorithm described in Section 2.4.1 [41]. The obtained apodization profile is plotted in Figure 7a. The synthesized grating device was readily feasible with existing fabrication methods, in terms of effective length, maximum refractive index modulation and average spatial resolution of the ripples in the apodization profile. A comparison between the fabrication-constrained spectral response in amplitude and phase with the originally defined response is shown in Figure 7b.

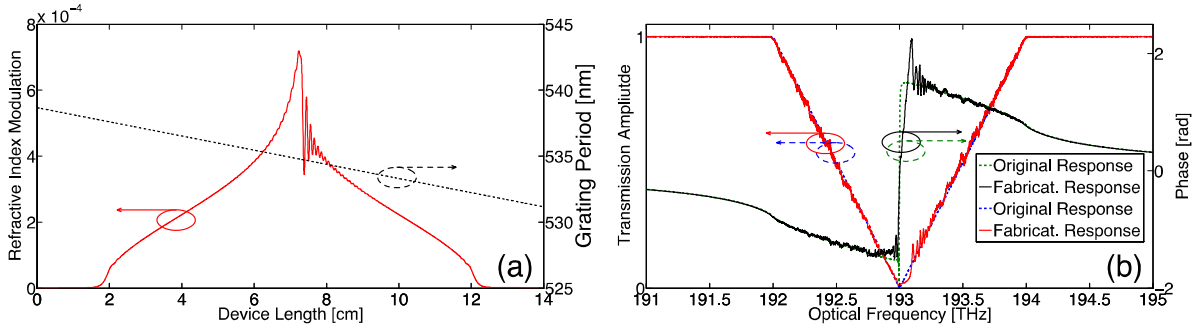

Figure 7. First-order optical differentiator based on a transmissive FBG: (**a**) Grating period (black dashed line) and apodization (red solid line) profiles considering linearly chirped phase mask and representative spatial resolution (0.3 mm); (**b**) Targeted transmission spectral response, phase (dotted green line) and amplitude (dotted blue line) and corresponding spectral response limited to fabrication constraints, in phase (solid black line) and amplitude (solid red line).

Figure 8 presents the output temporal characterization for the first-order optical differentiator as well as their performance based on the correlation coefficient and the TBP. Thus, Figure 8a shows the comparison between the ideally expected output waveform and the output from an FBG tailored to typical fabrication constraints. The two curves show an excellent match. Besides, Figure 8b shows the comparison in performance between the original designed spectral response and the fabrication-constrained spectral response.

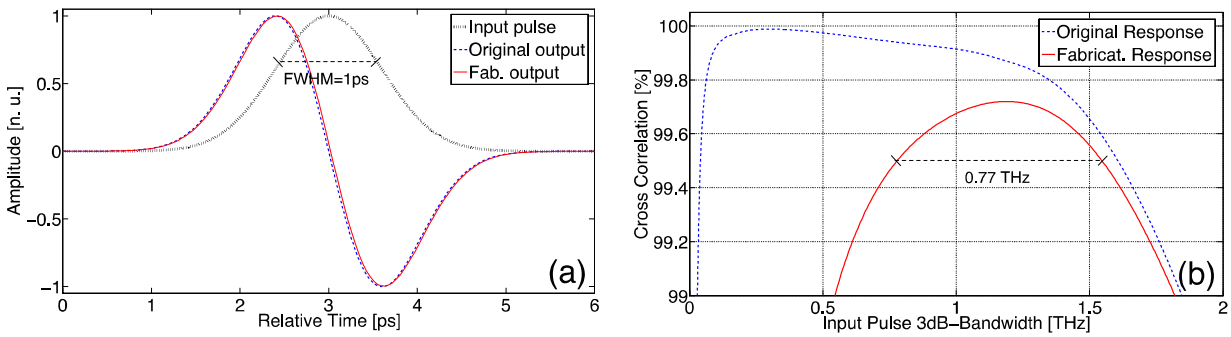

Figure 8. (**a**) Input Gaussian pulse (dotted black line), output of an ideal first-order differentiator (dashed blue line) and output of a first-order differentiator based on a fabrication-constrained FBG in transmission (red solid line); (**b**) Cross-correlation coefficient as a function of the 3 dB-bandwidth of the input pulse for the original design (blue dashed line) and the design tailored to fabrication constraints (red solid line).

The FBG-based optical differentiator performance is mainly degraded for inputs whose bandwidth is below 0.5 THz, while preserving an excellent behavior for input pulses with a 3 dB-bandwidth ranging between 0.78 and 1.55 THz. This fact translates into a TBP~2 calculated as the ratio between the maximum and the minimum input pulse 3dB-bandwidth with C_C higher than 99.5%). This degradation is predominantly attributed to imperfections of the fabrication-constrained device spectral response nearby the transmission resonance notch.

Higher order (up to $N = 4$) optical differentiators with optical bandwidth of 2 THz were also designed based on the same technique [61]. Results are depicted in Figure 9. Numerical simulations are employed to assess the output temporal waveforms when an input pulse, Gaussian-like, with 850 fs-FWHM is considered. The first- to-fourth order derivatives of the input pulse are shown in Figure 9b, where the output of the ideal differentiators are also depicted in black, validating their excellent operation.

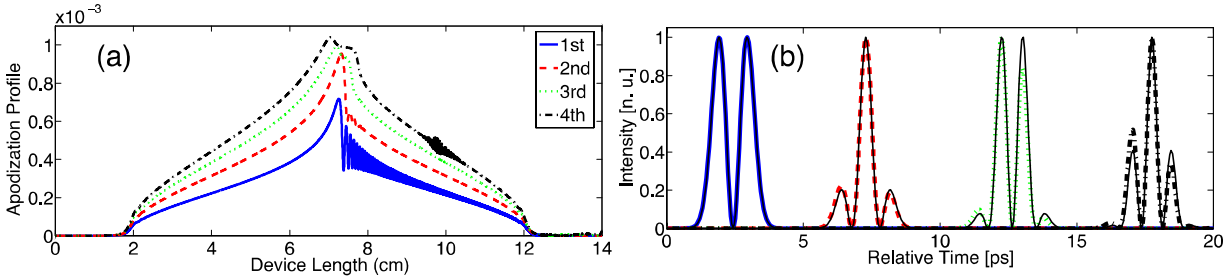

Figure 9. (**a**) Apodization profiles of the gratings required to implement Nth-order (up to N = 4) optical differentiators based on FBGs in transmission considering realistic spatial resolution (0.5 mm); (**b**) Intensity outputs from the obtained FBG devices.

High-order differentiators and fractional-order differentiators (i.e., those in which the parameter N is not an integer number) have been also presented based on FBGs in transmission, but obtaining a smart-engineered apodization phase modulation, based on a two-step nonlinear optimization algorithm, instead of a linear chirp [62,63].

3.3. Optical Integrators

FBG technology has served as a platform to implement another important all-optical signal processor, namely the optical integrator [64]. An optical integrator provides the cumulative time integral of the complex temporal envelope of an input optical signal. Its transfer function is

$$y(t) \propto \int_{\tau_N=-\infty}^{t} , \cdots , \int_{\tau_1}^{\tau_2} x(\tau_1) d\tau_1 d\tau_2 \cdots d\tau_N \rightarrow H_{\text{int}}(f) \propto \frac{1}{(j \cdot (f - f_0))^N} \tag{43}$$

Among the applications of FBG-based optical integrators proposed in the literature, we can highlight the implementation of unit-step time-domain waveforms and the generation of flat-top pulse shapers, enabling re-configurability of their temporal width. Additionally, they are also key components for solving ODEs, with much better performance in terms of high-frequency noise than optical differentiators [5]. Generally speaking, an optical integrator can be interpreted as the light-wave equivalent of an electronic capacitor. The main drawback of any passive temporal integrator is that it necessarily operates over a limited time window, due to practical design and fabrication constraints [65].

Significant efforts have been devoted to the implementation of broadband, high-resolution arbitrary order (Nth) optical integrators. Solutions based on passive and active configurations have been theoretically proposed based on FBGs in reflection and transmission, while some of them have been also experimentally demonstrated [64–71]. The first approach was based on FBG analysis algorithms using a phase-shifted FBG in transmission as an optical temporal integrator [64] with operation bandwidths in the order of tens of GHz. Subsequently, from temporal specifications and based on the first-order Born approximation, an uniform FBG operating in reflection was proposed as a first-order temporal integrator over a limited time window [65]. This implementation was later generalized to high-order temporal integrators using a weak-coupling uniform FBG with a proper apodization function [67–69]. Finally, these FBG-based optical integrator designs operating in reflection were optimized by means of strong-coupling uniform FBGs (using FBG synthesis algorithms), increasing their energy efficiency and processing accuracy. Experimental results were presented in [70,71].

3.4. Photonic Hilbert Transformers

FBG-based photonic Hilbert transformers (PHT), also known as phase shifters, have been also proposed and experimentally demonstrated based on FBGs working in reflection [72–77] and transmission [78,79]. A PHT is a pulse processor that delivers the Hilbert transform of an input optical pulse. The transfer function of a general PHT is defined as

$$y(t) \propto H^{(P)}[x(t)] \rightarrow H_{PHT}(f) \propto \cos(\varphi) + \sin(\varphi) \times (-j \cdot sign(f - f_0)) \quad (44)$$

where H represents Hilbert transformation, $\varphi = P \cdot \pi/2$, and P is the fractional order, being P a real number. The PHT is called integer when $P = 1$. PHTs are important components for a high number of applications in the fields of computing and communications. As optical signal processors, PHTs have been employed in the generation of phase-shifted pulse doublets, where the PHT order allows one to define the amplitude ratio between the pulse lobes. They have been also proposed to implement single side-band modulation from amplitude modulation formats [76].

The first approach to the design of an FBG-based integer PHT was based on a weak-coupling uniform FBG (using the first-order Born approximation) with a properly designed amplitude-only grating apodization profile incorporating a single phase shift in the middle of the grating length [72]. The generalization for higher- and fractional-order PHTs were proposed based on strong-coupling uniform FBGs using grating synthesis algorithms [74,75]. Practical fabrication constraints imposed operation bandwidths typically in the order of 200 GHz.

To overcome this bandwidth limitation, FBG-based PHTs in transmission mode have been proposed taking into account that the PHT transfer function in not minimum phase [42]. By following the design approach presented in Section 2.4.2, two Hilbert transformers with an operation bandwidth of 3 THz, i.e., an integer, i.e., $P = 1$ and a fractional one, $P = 0.81$, were experimentally demonstrated [78]. As in previous processors based on FBGs in transmission, the grating profile (apodization and phase) were readily feasible, even for a relatively strong-coupling grating. Figure 10a,b shows the reflectivity and group delay in reflection of the integer HT, comparing the ideal and the experimentally measured curves. The reflectivity follows the anticipated interferogram-like profile described in Section 2.4.2. In particular, the target discrete shift in the phase spectral response of the PHT is encoded as the phase shift in the middle of the sinusoidal interferogram profile, while the all-pass PHT filter response imposes the nearly uniform interferogram envelope.

The signal at the output of the PHTs are represented in Figure 10c,d. The experimentally obtained Hilbert-transformed output component of the fabricated devices when the input pulse is Gaussian-like and has an FWHM (Full-Width Half-Maximum) of 0.88 ps are presented in Figure 10c,d, with the corresponding simulated outputs for comparative purposes, showing a fairly good match in both cases. Some deviations are attributed to the low signal-to-noise ratio of the measured signals as a result of the application of a Fourier transform spectral interferometry procedure for the pulse characterization [42].

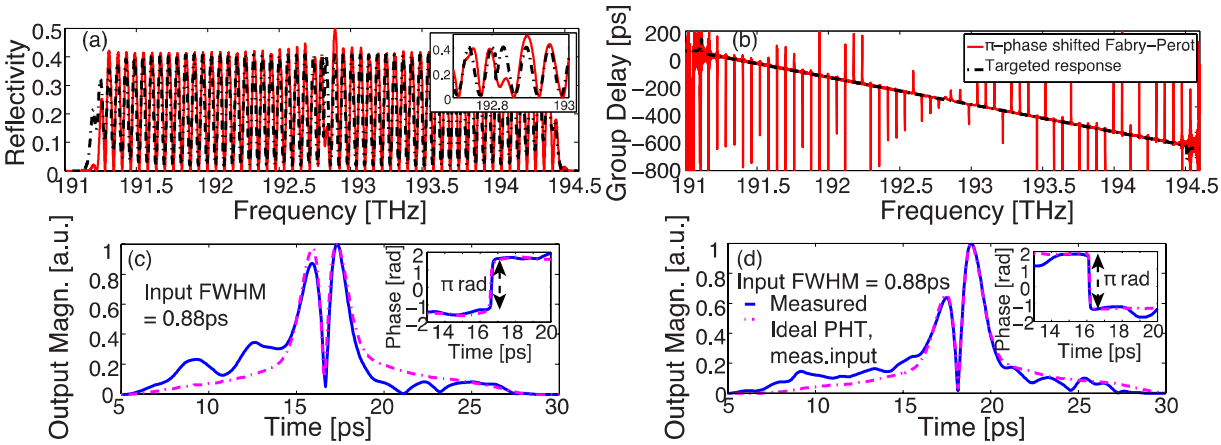

Figure 10. PHT implemented in an FBG in transmission: Comparison between the specified reflectivity (**a**) and group delay (**b**) (in dashed black line) and the experimentally implemented structure (in solid red). Comparison between the experimentally obtained output component of the fabricated integer (**c**) and fractional (**d**) PHTs (solid blue line) and the ideal output (dashed pink line) for an input Gaussian pulse with 0.88 ps-FWHM.

3.5. Optical Pulse-Shapers

Optical pulse shapers are devices that synthesize the user-defined shape of the complex-valued time-domain envelope of an optical wave. Pulse shapers play a fundamental role in computation and communication systems [80]. The more direct approach of using FBGs as a pulse-shaping processor consists of employing the first-order Born approximation [81–85]. As significant examples of this design approach, we can mention the implementation of flat-top [81,82], saw-tooth (triangular) [83], parabolic [84] and antisymmetric Hermite-Gauss [85] pulse shapers. These kinds of pulse-shaping processors permit the synthesis of a wide variety of important ultra-fast optical signal processing operations. Among them, we can mention the following: flat-top waveforms can be employed as all-optical control signals in nonlinear switching procedures; parabolic pulses can be used as pump signals in all-optical non-linear implementations of time-lens processes or pulse retiming; triangular waveforms can be used to implement tunable delay lines, time-domain add-and-drop multiplexers, wavelength converters, or doubling of optical signals; sinc-shape are used in optical time division multiplexing (OTDM) systems with Nyquist pulse shaping; and the generation of high-order modulation codes are necessary for optical code-division multiple access (OCDMA) and optical-label-switching communications.

Based on grating analysis algorithms, applications of ultrashort pulse propagation in FBG were proposed for DWDM and OCDMA [86]. Different approaches have been proposed in the literature. For example, arrays of uniform FBGs have been utilized for generation of bipolar codes. In addition, schemes relying on superstructured FBGs, or step-chirped FBGs were also presented, representing more compact solutions [87–91]. Based on grating synthesis algorithms, a flat-top pulse-shaper based on uniform FBG operating in transmission was proposed with an operation bandwidth in the order of tens of GHz (but with a very complex refractive index profile with high peaks and several precisely distributed phase shifts) [92]. Later, rectangular, parabolic and triangular pulse shapers based on phase-modulated FBGs in transmission have been proposed using grating synthesis

algorithms and numerical optimization [93]. More in particular, a method is employed that is based on finding a suitable period profile $\Lambda(z)$ that attains the target transmissive spectral response from the FBG, while the apodization profile remains constant. This technique implies a simpler grating writing process, as the coupling strength remains constant along most of the device length. However, the complexity is transferred to the fabrication of the phase mask, which now needs to have a user-defined, relatively complex shape.

The aforementioned implementations for FBG-based all-optical pulse shapers present a limited operation bandwidth (i.e., of hundreds of GHz, as explained in Section 2.4). The implementation of optical pulse shapers using FBG operating in transmission, following the design approach presented in Section 2.4.1, raised particular interest for increasing the operation bandwidth. In general, any pulse shaping functionality can be implemented using this configuration provided that its transfer function is minimum-phase. By using this configuration, a 5 THz bandwidth flat-top pulse shaper has been experimentally demonstrated [94]. The synthesized grating profile obtained from this design approach, shown in Figure 11a, is much simpler than that obtained from previous approaches and readily feasible, even for a strong coupling grating. Figure 11c shows the measured spectrum of the input optical pulse. Figure 11d presents the measured transmissive power spectral response for the FBG-based pulse shaper, and Figure 11e the corresponding measured spectral phase response.

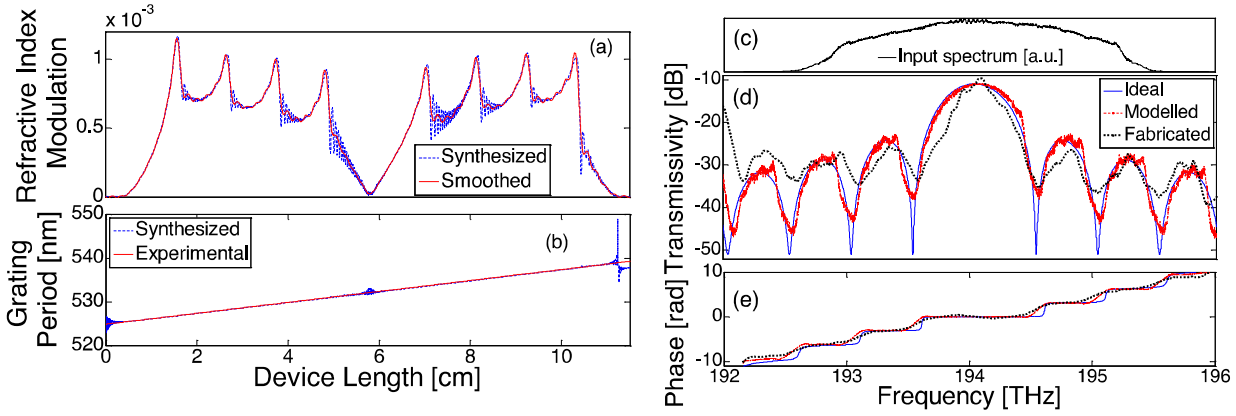

Figure 11. Apodization profile (**a**) and period (**b**) of a rectangular pulse-shaper implemented on an FBG in transmission. The curves obtained from the synthesis algorithm are in blue, while smoothed profiles adapted to the restrictions of the fabrication method (sub-mm resolution) are in red; (**c**) Spectrum of the experimental input signal; (**d**) transmissivity and (**e**) ideal phase of the spectral response in transmission (blue line), analytical response restrained to fabrication limitations (red line) and experimentally measured response (dotted black line).

For the FBG-based pulse shaper temporal characterization, the output signal is measured in amplitude and phase via Fourier transform spectral interferometry. The input (a 400 fs-FWHM Gaussian pulse) and the output time-domain signals are plotted in Figure 12. The experimentally obtained data and the ideally expected data are compared in that figure, showing high similarity and hence verifying the ability of the fabricated FBG to attain the target ultrafast pulse-shaping application.

More recently, it has been presented the possibility of using FBGs with orthogonal impulses responses to perform coding operations aimed at implementing multidimensional quantum key distribution (QKD) protocols overcoming the low secret-key rate for quantum information processing [95].

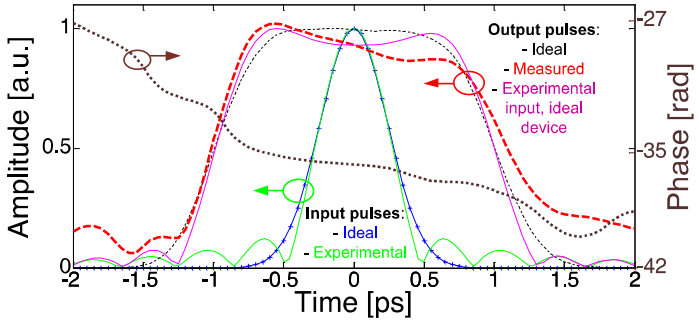

Figure 12. Ideal temporal input pulse (blue line) and pulse employed in the characterization of a flat-top pulse shaper implemented on a FBG in transmission (green line); Ideal temporal output (black line) and experimentally measured output (red line). The output signal from the input employed in the experimental test (green line) and the ideal device response is also plotted (magenta line), to show deviations from the ideal output owing to the employed pulse.

4. Discussion

In the past two decades, much research has been carried out in the development of all optical signal processors with high bandwidth (even up to the THz regime), aimed at replacing the currently employed electronic processors. Methods for performing analysis and synthesis of FBG enabled the development of a myriad of different filters and optical pulse processors based on FBG technology. This research line was highly fruitful along the first 15 years of this century. From 2016, the research interest in FBG as signal processors started to decrease. The use of optical processors in a fiber platform is currently limited to dispersion compensation devices based on linearly-chirped FBGs, and band pass filtering components (i.e., those described in Section 3.1). Nowadays, the interest on these processing components is mainly focused on the development of Bragg gratings in integrated platforms. In particular, the need for particular filtering operations to implement complete functionalities on a chip, e.g., in microwave photonics processors, beamforming networks, arbitrary waveform generation, etc. is widely recognized [18–20,96]. The development of optical processors on integrated Bragg gratings is following a similar path to the one that occurred in fiber platforms. At present, most of the implemented functionalities have been developed via approximations. Recently, analysis tools have been formulated with the aim to predict the effect of particular apodization or period variations on the grating spectral response prior the fabrication of the devices [97]. The next natural step is the development of synthesis tools that enable the design of energy efficient, high precise spectral filtering responses in integrated waveguide Bragg gratings. The design tools described in this review paper can serve as a baseline for the development of the required tools in integrated platforms.

Through the years, one of the most criticized features of FBG has been the difficulty in producing reconfigurable processors. When talking about reconfigurability, we not only mean the processing operation, but also the features related to their performance, e.g., the fact that the processor can be employed to produce output waveforms with different temporal features. The only parameter that is relatively simple to alter is the central frequency of operation, which is dependent on the temperature or the strain on the structure. Based on the possibility of altering the operation frequency of the grating, there have been attempts to attain programmable and reconfigurable components [98–100]. An example is the development of a second order optical differentiator based on linearly chirped FBG and a digital thermal print head [100]. Advances towards reconfigurable structures are being researched nowadays through the use of innovative methods for modifying the grating physical parameters in a programmable means or by using static FBGs in more complex interferometric schemes, even in integrated platforms [101].

5. Conclusions

In this work, we have presented a wide revision of the literature on fiber Bragg gratings for their use as analog all-optical signal processors. Two main objectives have been pursued in the preparation of this manuscript. First, to collect the different approaches to perform the design of optical linear filters based on FBG technology. For this purpose, we have classified the existing methodologies into analysis and synthesis tools, and we have described their fundamentals, including those based on coupled-mode theory and on multi-layer methods. Then, we have revisited the main optical processing units that have been implemented via FBGs, providing a brief idea of their potential applications. Of course, optical fiber technology has been nothing but a platform for the development of these optical signal processors. Current trends move towards the headway of these processors on Bragg gratings in integrated platforms. The ultimate goal is the replacement of electronic-based processors, hence avoiding the operation bandwidth bottlenecks and the inefficient OE-EO conversion associated with their use.

Author Contributions: These authors contributed equally to this work. Both authors have read and agreed to the published version of the manuscript.

Funding: This research received no external funding.

Acknowledgments: The authors want to acknowledge José Azaña for the interesting discussions and for his contributions to many of the signal processing units here reviewed.

Conflicts of Interest: The authors declare no conflict of interest.

References

1. Hill, K.; Meltz, G. Fiber Bragg grating technology fundamentals and overview. *J. Light. Technol.* **1997**, *15*, 1263–1276. [CrossRef]
2. Othonos, A.; Kalli, K.; Kohnke, G.E. Fiber Bragg Gratings: Fundamentals and Applications in Telecommunications and Sensing. *Phys. Today* **2000**, *53*, 61–62. [CrossRef]
3. Kashyap, R. *Fiber Bragg Gratings*, 2nd ed.; Academy Press: San Diego, CA, USA, 2009.
4. Giles, C. Lightwave applications of fiber Bragg gratings. *J. Light. Technol.* **1997**, *15*, 1391–1404. [CrossRef]
5. Azaña, J. Ultrafast Analog All-Optical Signal Processors Based on Fiber-Grating Devices. *IEEE Photonics J.* **2010**, *2*, 359–386. [CrossRef]
6. Erdogan, T. Fiber grating spectra. *J. Lightwave Technol.* **1997**, *15*, 1277–1294. [CrossRef]
7. Yin, S.; Rufin, P.B.; Yu, F.T.S. *Fiber Optic Sensor*, 2nd ed.; CRC Press: Boca Raton, FL, USA, 2008.
8. Udd, E.; Spillman, W.B. *Fiber Optic Sensors: An Introduction for Engineer and Scientists*, 2nd ed.; John Wiley & Sons: UK, 2011.
9. Willner, A.E.; Khaleghi, S.; Reza Chitgarha, M.; Faruk Yilmaz, O. All-Optical Signal Processing. *J. Lightwave Technol.* **2014**, *32*, 660–680. [CrossRef]
10. Wabnitz, S.; Eggleton, B.J. *All-Optical Signal Processing*; Springer: New York, NY, USA, 2015.
11. Kersey, A.D.; Davis, M.A.; Patrick, H.J.; LeBlanc, M.; Koo, K.P.; Askins, C.G.; Putnam, M.A.; Friebele, E.J. Fiber grating sensors. *J. Lightwave Technol.* **1997**, *15*, 1442–1463. [CrossRef]
12. Moyo, P.; Brownjohn, J.M.W.; Suresh, R.; Tjin, S.C. Development of fiber Bragg grating sensors for monitoring civil infra-structure. *Eng. Struct.* **2005**, *27*, 1828–1834. [CrossRef]
13. Kinet, D.; Mégret, P.; Goossen, K.W.; Qiu, L.; Heider, D.; Caucheteur, C. Fiber Bragg Grating Sensors toward Structural Health Monitoring in Composite Materials: Challenges and Solutions. *Sensors* **2014**, *14*, 7394–7419. [CrossRef] [PubMed]
14. Ma, Z.; Chen, X. Fiber Bragg Gratings Sensors for Aircraft Wing Shape Measurement: Recent Applications and Technical Analysis. *Sensors* **2018**, *19*, 55. [CrossRef]
15. Zhao, W.; Zhong, K.; Chen, W. A Fiber Bragg Grating Borehole Deformation Sensor for Stress Measurement in Coal Mine Rock. *Sensors* **2020**, *20*, 3267. [CrossRef]
16. Sahota, J.; Gupta, N.; Dhawan, D. Fiber Bragg grating sensors for monitoring of physical parameters: A comprehensive review. *Opt. Eng.* **2020**, *59*, 060901. [CrossRef]
17. Fernández-Ruiz, M.R.; Carballar, A.; Ashrafi, R.; LaRochelle, S.; Azaña, J. All-Optical Pulse Shaping in the Sub-Picosecond Regime Based on Fiber Grating Devices. *Shap. Light Nonlinear Opt. Fibers* **2017**, *9*, 257–292. [CrossRef]
18. Burla, M.; Romero-Cortés, L.; Li, M.; Wang, X.; Chrostowski, L.; Azaña, J. Integrated waveguide Bragg gratings for micro-wave photonics signal processing. *Opt. Express* **2013**, *21*, 25120–25147. [CrossRef] [PubMed]
19. Lui, W. Ultra-Fast Photonic Signal Processors based on Photonic Integrated Circuits. Ph.D. Thesis, University of Otawa, Otawa, ON, Canada, 2017.
20. Kaushal, S.; Cheng, R.; Ma, M.; Mistry, A.; Burla, M.; Chrostowski, L.; Azaña, J. Optical signal processing based on silicon photonics waveguide Bragg gratings: Review. *Front. Optoelectron.* **2018**, *11*, 163–188. [CrossRef]

21. Oppenheim, A.V.; Schafer, R.W. *Discrete-Time Signal Processing*; Prentice-Hall: Upper Saddle River, NJ, USA, 1989.
22. Poladian, L. Group-delay reconstruction for fiber Bragg gratings in reflection and transmission. *Opt. Lett.* **1997**, *22*, 1571–1573. [CrossRef]
23. Carballar, A.; Muriel, M.A. Phase reconstruction from reflectivity in fiber Bragg gratings. *J. Light. Technol.* **1997**, *15*, 1314–1322. [CrossRef]
24. Mecozzi, A. Retrieving the full optical response from amplitude data by Hilbert transform. *Opt. Commun.* **2009**, *282*, 4183–4187. [CrossRef]
25. Miller, S.E. Coupled Wave Theory and Waveguide Applications. *Bell Syst. Tech. J.* **1954**, *33*, 661–719. [CrossRef]
26. Delano, E. Fourier Synthesis of Multilayer Filters*. *J. Opt. Soc. Am.* **1967**, *57*, 1529–1532. [CrossRef]
27. Yariv, A. Coupled-mode theory for guided-wave optics. *IEEE J. Quantum Electron.* **1973**, *9*, 919–933. [CrossRef]
28. Kogelnik, H. Filter Response of Nonuniform Almost-Periodic Structures. *Bell Syst. Tech. J.* **1976**, *55*, 109–126. [CrossRef]
29. Muriel, M.A.; Carballar, A. Internal field distributions in fiber Bragg gratings. *IEEE Photonics Technol. Lett.* **1997**, *9*, 955–957. [CrossRef]
30. Muriel, M.A.; Carballar, A.; Azana, J. Field distributions inside fiber gratings. *IEEE J. Quantum Electron.* **1999**, *35*, 548–558. [CrossRef]
31. Macleod, H.A. *Thin-Film Optical Filters*, 3th ed.; Institute of Physics Publishing: London, UK, 2002.
32. Capmany, J.; Muriel, M.A.; Sales, S.; Rubio, J.; Pastor, D.; Daniel, P. Microwave V-I transmission matrix formalism for the analysis of photonic circuits: Application to fiber Bragg gratings. *J. Light. Technol.* **2003**, *21*, 3125–3134. [CrossRef]
33. Yeh, P.; Hendry, M. Optical Waves in Layered Media. *Phys. Today* **1990**, *43*, 77–78. [CrossRef]
34. Peral, E.; Capmany, J.; Marti, J. Iterative solution to the Gel'Fand-Levitan-Marchenko coupled equations and application to synthesis of fiber gratings. *IEEE J. Quantum Electron.* **1996**, *32*, 2078–2084. [CrossRef]
35. Feced, R.; Zervas, M.N.; Muriel, M.A. An efficient inverse scattering algorithm for the design of nonuniform fiber Bragg gratings. *IEEE J. Quantum Electron.* **1999**, *35*, 1105–1115. [CrossRef]
36. Poladian, L. Simple grating synthesis algorithm. *Opt. Lett.* **2000**, *25*, 787–789. [CrossRef]
37. Skaar, J.; Wang, L.; Erdogan, T.; Skaar, J.; Wang, L.; Erdogan, T. On the synthesis of fiber Bragg gratings by layer peeling. *IEEE J. Quantum Electron.* **2001**, *37*, 165–173. [CrossRef]
38. Skaar, J. Synthesis of fiber Bragg gratings for use in transmission. *J. Opt. Soc. Am. A* **2001**, *18*, 557–564. [CrossRef]
39. Azaña, J.; Chen, L.R. Synthesis of temporal optical waveforms by fiber Bragg gratings: A new approach based on space-to-frequency-to-time mapping. *J. Opt. Soc. Am. B* **2002**, *19*, 2758–2769. [CrossRef]
40. Capmany, J.; Muriel, M.A.; Sales, S. Synthesis of 1D Bragg gratings by a layer-aggregation method. *Opt. Lett.* **2007**, *32*, 2312–2314. [CrossRef] [PubMed]
41. Ruiz, M.D.R.F.; Carballar, A.; Azaña, J. Design of Ultrafast All-Optical Signal Processing Devices Based on Fiber Bragg Gratings in Transmission. *J. Light. Technol.* **2013**, *31*, 1593–1600. [CrossRef]
42. Ruiz, M.D.R.F.; Carballar, A.; Azana, J. Arbitrary Time-Limited Optical Pulse Processors Based on Transmission Bragg Gratings. *IEEE Photonics Technol. Lett.* **2014**, *26*, 1754–1757. [CrossRef]
43. Sklar, B. *Digital Communications. Fundamentals and Applications*; Prentice Hall: Upper Saddle River, NJ, USA, 1988.
44. Andre, P.S.; Pinto, A.N.; Pinto, J.L.; Almeida, T.; Pousa, M. *Tunable Transparent and Cost Effective Optical Add-Drop Multi-Plexer Based on Fiber Bragg Grating for DWDM Networks. 2001 Digest of LEOS Summer Topical Meetings: Advanced Semi-conductor Lasers and Applications/Ultraviolet and Blue Lasers and Their Applications/Ultralong Haul DWDM Transmission and Networking/WDM Compo*; IEEE: Copper Mountain, CO, USA, 2001.
45. Canning, J.; Psaila, D.C.; Brodzeli, Z.; Higley, A.; Janos, M. Characterization of apodized fiber Bragg gratings for rejection filter applications. *Appl. Opt.* **1997**, *36*, 9378–9382. [CrossRef] [PubMed]
46. Ibsen, M.; Feced, R.; Petropoulos, P.; Zervas, M.N. 99.9% reflectivity dispersion-less square-filter fibre Bragg gratings for high speed DWDM networks. Optical Fiber Communication Conference. Technical Digest Postconference Edition. *Trends Opt. Photonics* **2002**, *4*, 230–232. [CrossRef]
47. Zhou, X.; Liang, G.; Wang, T. An optical add-drop multiplexer design based on fiber Bragg gratings. In Proceedings of the 2011 International Conference on Electronics and Optoelectronics, Dalian, China, 29–31 July 2011; Volume 2, pp. 41–43.
48. Hill, K.O.; Takiguchi, K.; Bilodeau, F.; Malo, B.; Kitagawa, T.; Thériault, S.; Johnson, D.C.; Albert, J. Chirped in-fiber Bragg gratings for compensation of optical-fiber dispersion. *Opt. Lett.* **1994**, *19*, 1314–1316. [CrossRef]
49. Muriel, M.A.; Azaña, J.; Carballar, A. Real-time Fourier transformer based on fiber gratings. *Opt. Lett.* **1999**, *24*, 1–3. [CrossRef]
50. Kolner, B. Space-time duality and the theory of temporal imaging. *IEEE J. Quantum Electron.* **1994**, *30*, 1951–1963. [CrossRef]
51. Guan, P.; Røge, K.M.; Lilllieholm, M.; Hu, H.; Galili, M.; Morioka, T.; Oxenløwe, L.K. Optical Signal Processing using Time Lens based Optical Fourier Transformation. In Proceedings of the Asia Communications and Photonics Conference 2016, Wuhan, China, 2–5 November 2016.
52. Ngo, N.Q.; Yu, S.F.; Tjin, S.C.; Kam, C.H. A new theoretical basis of high-derivative optical differentiators. *Opt. Commun.* **2004**, *230*, 115–129. [CrossRef]
53. Park, Y.; Slavík, R.; Azaña, J. Ultrafast all-optical differentiators for generation of orthogonal (sub-) picosecond Her-mite-Gaussian waveforms. In Proceedings of the Optical Fiber Communication (OFC), Anaheim, CA, USA, 25–29 March 2007. Abstract Number OThI2.

54. Berger, N.K.; Levit, B.; Fischer, B.; Kulishov, M.; Plant, D.V.; Azaña, J. Temporal differentiation of optical signals using a phase-shifted fiber Bragg grating. *Opt. Express* **2007**, *15*, 371–381. [CrossRef]
55. Kulishov, M.; Azaña, J. Desing of high-order all-optical temporal differentiators based on multiple-phase-shifted fiber Bragg gratings. *Opt. Express* **2007**, *15*, 6152–6166. [CrossRef] [PubMed]
56. Rivas, L.M.; Singh, K.; Carballar, A.; Azana, J. Arbitrary-Order Ultrabroadband All-Optical Differentiators Based on Fiber Bragg Gratings. *IEEE Photonics Technol. Lett.* **2007**, *19*, 1209–1211. [CrossRef]
57. Preciado, M.A.; Muriel, M.A. Design of an ultrafast all-optical differentiator based on a fiber Bragg grating in transmission. *Opt. Lett.* **2008**, *33*, 2458–2460. [CrossRef]
58. Li, M.; Janner, D.; Yao, J.; Pruneri, V. Arbitrary-order all-fiber temporal differentiator based on a fiber Bragg grating: Design and experimental demonstration. *Opt. Express* **2009**, *17*, 19798–19807. [CrossRef]
59. Gatti, D.; Fernandez, T.; Longhi, S.; Laporta, P. Temporal differentiators based on highly-structured fibre Bragg gratings. *Electron. Lett.* **2010**, *46*, 943–945. [CrossRef]
60. Preciado, M.A.; Xu, X.; Harper, P.; Sugden, K. Experimetal demonstration of an optical differentiator based on a fiber Bragg grating in transmission. *Opt. Lett.* **2013**, *38*, 917–919. [CrossRef]
61. Fernandez-Ruiz, M.R.; Azaña, J.; Carballar, A. Ultra-fast all-optical Nth-order Differentiators based on transmission fiber Bragg gratings. In Proceedings of the IEEE Photonics Conference 2012, San Francisco, CA, USA, 18 May 2012; pp. 656–657.
62. Liu, X.; Shu, X. Design of an all-optical fractional-order differentiator with terahertz bandwidth based on a fiber Bragg grating in transmission. *Appl. Opt.* **2017**, *56*, 6714–6719. [CrossRef]
63. Liu, X.; Shu, X. Design of arbitrary-order photonic temporal differentiators based on phase-modulated fiber Bragg gratings in transmission. *J. Light. Technol.* **2017**, *35*, 2926–2932. [CrossRef]
64. Ngo, N.Q. Design of an optical temporal integrator based on a phase-shifted fiber Bragg grating in transmission. *Opt. Lett.* **2007**, *32*, 3020–3022. [CrossRef]
65. Azaña, J. Proposal of a uniform fiber Bragg grating as an ultrafast all-optical integrator. *Opt. Lett.* **2007**, *33*, 4–6. [CrossRef]
66. Preciado, M.A.; Muriel, M.A. Ultrafast all-optical integrator based on a fiber Bragg grating: Proposal and design. *Opt. Lett.* **2008**, *33*, 1348–1350. [CrossRef] [PubMed]
67. Asghari, M.H.; Azaña, J. Design of all-optical high-order temporal integrators based on multiple-phase-shifted Bragg gratings. *Opt. Express* **2008**, *16*, 11459–11469. [CrossRef]
68. Park, Y.; Ahn, T.-J.; Dai, Y.; Yao, J.; Azaña, J. All-optical temporal integration of ultrafast pulse waveforms. *Opt. Express* **2008**, *16*, 17817–17825. [CrossRef]
69. Slavík, R.; Park, Y.; Ayotte, N.; Doucet, S.; Ahn, T.-J.; LaRochelle, S.; Azaña, J. Photonic temporal integrator for all-optical computing. *Opt. Express* **2008**, *16*, 18202–18214. [CrossRef]
70. Asghari, M.H.; Azana, J.; Azaa, J. On the Design of Efficient and Accurate Arbitrary-Order Temporal Optical Integrators Using Fiber Bragg Gratings. *J. Light. Technol.* **2009**, *27*, 3888–3895. [CrossRef]
71. Wang, C.; Yao, J.; Azaña, J. High-order passive photonic temporal integrators. *Opt. Lett.* **2010**, *35*, 1191–1193. [CrossRef]
72. Asghari, M.H.; Azaña, J. All-optical Hilbert transformer based on a single phase-shifted fiber Bragg grating: Design and analysis. *Opt. Lett.* **2009**, *34*, 334–336. [CrossRef]
73. Cuadrado-Laborde, C. Proposal and Design of a Photonic In-Fiber Fractional Hilbert Transformer. *IEEE Photonics Technol. Lett.* **2009**, *22*, 33–35. [CrossRef]
74. Li, M.; Yao, J. All-fiber temporal photonic fractional Hilbert transformer based on a directly designed fiber Bragg grating. *Opt. Lett.* **2010**, *35*, 223–225. [CrossRef]
75. Li, M.; Yao, J. Experimental Demonstration of a Wideband Photonic Temporal Hilbert Transformer Based on a Single Fiber Bragg Grating. *IEEE Photonics Technol. Lett.* **2010**, *22*, 1559–1561. [CrossRef]
76. Li, Z.; Chi, H.; Zhang, X.; Yao, J. Optical Single-Sideband Modulation Using a Fiber-Bragg-Grating-Based Optical Hilbert Transformer. *IEEE Photonics Technol. Lett.* **2011**, *23*, 558–560. [CrossRef]
77. Carballar, A.; Fernández-Ruiz, M.R.; Azaña, J. Design of photonic Hilbert transformers based on impulsive response specifications. In Proceedings of the IEEE Photonics Conference (IPC), Reston, VA, USA, 4–8 October 2015.
78. Fernández-Ruiz, M.R.; Wang, L.; Carballar, A.; Burla, M.; Azaña, J.; LaRochelle, S. THz-bandwidth photonic Hilbert trans-formers based on fiber Bragg gratings in transmission. *Opt. Lett.* **2015**, *40*, 41–44. [CrossRef] [PubMed]
79. Li, Y.; Liu, X.; Shu, X.; Zhang, L. Arbitrary-Order Photonic Hilbert Transformers Based on Phase-Modulated Fiber Bragg Gratings in Transmission. *Photonics* **2021**, *8*, 27. [CrossRef]
80. Weiner, A.M. Ultrafast optical pulse shaping: A tutorial review. *Opt. Commun.* **2011**, *284*, 3669–3692. [CrossRef]
81. Petropoulos, P.; Ibsen, M.; Ellis, A.; Richardson, D. Rectangular pulse generation based on pulse reshaping using a superstructured fiber Bragg grating. *J. Light. Technol.* **2001**, *19*, 746–752. [CrossRef]
82. Parmigiani, F.; Petropoulos, P.; Ibsen, M.; Richardson, D.J. All-optical pulse reshaping and retiming systems incorporating pulse shaping fiber Bragg gratings. *J. Lightwave Technol.* **2006**, *19*, 357–364. [CrossRef]
83. Parmigiani, F.; Ibsen, M.; Ng, T.T.; Provost, L.; Petropoulos, P.; Richardson, D.J. An efficient wavelength converter exploiting a grating-based saw-tooth pulse shaper. *IEEE Photonics Technol. Lett.* **2008**, *20*, 1461–1463. [CrossRef]
84. Parmigiani, F.; Petropoulos, P.; Ibsen, M.; Richardson, D. Pulse retiming based on XPM using parabolic pulses formed in a fiber Bragg grating. *IEEE Photonics Technol. Lett.* **2006**, *18*, 829–831. [CrossRef]

85. Curatu, G.; LaRochelle, S.; Paré, C.; Bélanger, P.-A. Pulse shaping with a phase-shifted fiber Bragg grating for antisymmetric pulse generation. *Photonics West 2001 LASE* **2001**, *4271*, 213–221. [CrossRef]
86. Chen, L.R.; Benjamin, S.D.; Smith, P.W.E.; Sipe, J.E. Applications of ultrashort pulse propagation in Bragg gratings for wavelength-division multiplexing and code-division multiple access. *IEEE J. Quantum Electron.* **1998**, *34*, 2117–2129. [CrossRef]
87. Teh, P.C.; Petropoulos, P.; Ibsen, M.; Richardson, D.J. A comparative study of the performance of seven- and 63-chip otpical code-division multiple-access encoders and decoders based on superstructured fiber Bragg gratings. *J. Lightwave Technol.* **2001**, *19*, 1352–1365.
88. Teh, P.; Ibsen, M.; Lee, J.; Petropoulos, P.; Richardson, D. Demonstration of a four-channel WDM/OCDMA system using 255-chip 320-Gchip/s quarternary phase coding gratings. *IEEE Photonics Technol. Lett.* **2002**, *14*, 227–229. [CrossRef]
89. Ayotte, S.; Rochette, M.; Magne, J.; Rusch, L.; LaRochelle, S. Experimental verification and capacity prediction of FE-OCDMA using superimposed FBG. *J. Light. Technol.* **2005**, *23*, 724–731. [CrossRef]
90. Fang, X.; Wang, D.N.; Li, S. Fiber Bragg grating for spectral phase optical code-division multiple-access encoding and de-coding. *J. Opt. Soc. Am. B* **2003**, *20*, 1603–1610. [CrossRef]
91. Chen, L.R. *Optical Code—Division Multiple Access Enabled by Fiber Bragg Grating Technology*; CEC Press: Boca Raton, FL, USA, 2006.
92. Preciado, M.A.; Muriel, M.A. Flat-top pulse generation based on a fiber Bragg grating in transmission. *Opt. Lett.* **2009**, *34*, 752–754. [CrossRef] [PubMed]
93. Preciado, M.A.; Shu, X.; Sugden, K. Proposal and design of phase-modulated fiber gratings in transmission for pulse shaping. *Opt. Lett.* **2012**, *38*, 70–72. [CrossRef] [PubMed]
94. Fernández-Ruiz, M.R.; Li, M.; Dastmalchi, M.; Carballar, A.; LaRochelle, S.; Azaña, J. Picosecond optical signal processing based on transmissive fiber Bragg gratings. *Opt. Lett.* **2013**, *38*, 1247–1249. [CrossRef]
95. Djordjevic, I.B.B. FBG-Based Weak Coherent State and Entanglement-Assisted Multidimensional QKD. *IEEE Photonics J.* **2018**, *10*, 7600512. [CrossRef]
96. Khan, M.H.; Shen, H.; Xuan, Y.; Zhao, L.; Xiao, S.; Leaird, D.E.; Weiner, A.M.; Qi, M. Ultrabroad-bandwidth arbitrary radiofrequency waveform generation with a silicon photonic chip-based spectral shaper. *Nat. Photonics* **2010**, *4*, 117–122. [CrossRef]
97. Cheng, R.; Chrostowski, L. Spectral Design of Silicon Integrated Bragg Gratings: A Tutorial. *J. Light. Technol.* **2021**, *39*, 712–729. [CrossRef]
98. Mora, J.; Ortega, B.; Andres, M.; Capmany, J.; Cruz, J.; Pastor, D.; Sales, S. Tunable dispersion device based on a tapered fiber Bragg grating and nonuniform magnetic fields. *IEEE Photonics Technol. Lett.* **2003**, *15*, 951–953. [CrossRef]
99. Zhang, Z.; Tian, C.; Mokhtar, M.R.; Petropoulos, P.; Richardson, D.R.; Ibsen, M. Rapidly reconfigurable optical phase en-coder-decoders based on fiber Bragg gratings. *IEEE Photonics Technol. Lett.* **2006**, *18*, 1216–1218. [CrossRef]
100. Wang, R.; Lin, R.; Tang, M.; Zhang, H.; Feng, Z.; Fu, S.; Liu, D.; Shum, P.P. Electrically Programmable All-Fiber Structured Second Order Optical Temporal Differentiator. *IEEE Photonics J.* **2015**, *7*, 7101510. [CrossRef]
101. Zhang, W.; Yao, J. A fully reconfigurable waveguide Bragg grating for programmable photonic signal processing. *Nat. Commun.* **2018**, *9*, 1396. [CrossRef] [PubMed]